Sustainable Energy & Fuels

ROYAL SOCIETY OF CHEMISTRY

PAPER

Published on 06 July 2026

Check for updates

Cite this: *Sustainable Energy Fuels*, 2026, **10**, 3811

Flexible low-carbon dimethyl ether production *via* reversible solid oxide cells and sorption-enhanced synthesis

Dion Jakobs, †[ab] Mathis Heyer,†[ac] Jannik Bothe,[a] Johanna Güttler,[ad] Jan Pavšek [a] and Kaan Rehwasser *[a]

Received 28th January 2026
Accepted 25th June 2026

DOI: 10.1039/d6se00114a

rsc.li/sustainable-energy

The transition to sustainable chemical production necessitates processes capable of utilizing captured CO_2 and adapting to the volatility of renewable energy. This work proposes a flexible Reversible Solid Oxide Cell (RSOC) and Sorption-Enhanced DME Synthesis (SEDMES) process for sustainable dimethyl ether production. We employ a rigorous optimization framework to evaluate the process under real-world, hourly-resolved energy scenarios. The optimized system achieves net negative cradle-to-gate greenhouse gas emissions (−1.96 $kg_{CO_2\ eq}$ per kg_{DME}) and high exergetic efficiency (50.2%), significantly outperforming fossil-based benchmarks. Economically, the process yields break-even prices ranging from 3.11 € per kg to 3.83 € per kg depending on the electricity procurement scenario. Crucially, the integration of flexible design, process optimization, and scheduling strategies reduces production costs by up to 57% relative to a static, heuristically designed baseline, validating the proposed concept as a robust pathway for cost effective, next generation sustainable fuels.

1 Introduction

To transition to a sustainable chemical industry, modern chemical processes must move beyond steady-state and fossil based designs and embrace flexible operation aligned with variable renewable energy and renewable feedstocks.[1] This shift requires not only novel process designs, like those utilizing captured CO_2,[2] but also requires processes inherently designed for dynamic, flexible operation, moving beyond traditional steady-state assumptions.[3,4] Developing novel production routes that meet this dual challenge while ensuring economic viability under intermittent operation is a critical, unmet need for the sustainable fuels sector.[5]

A prime candidate for this sustainable redesign is dimethyl ether (DME).[6–10] As a versatile chemical and clean-burning fuel, sustainable DME production routes are actively being researched, often focusing on two distinct areas: novel feedstocks and advanced synthesis development. Research has meaningfully advanced both of these fronts, especially in the form of green feedstock utilization and improving process intensification.

Most fossil-free process designs for DME production aim to replace the fossil-based syngas input stream with renewable alternatives. This is frequently achieved by preceding the core synthesis pathway with biomass gasification,[11–15] electrolysis-based processes,[16–21] or combinations thereof.[22] For example, Pozzo *et al.*[22] propose a process where biomass is gasified to a CO_2-rich syngas, further enriched in CO and H_2 using a solid oxide electrolysis cell (SOEC), and finally converted to DME *via* direct DME synthesis. While efficient in heat integration, this design introduced challenges such as very low operating temperatures (−40 °C) and a complex DME purification procedure. Most other process proposals come at the cost of high pressures, significant recycle streams, and commonly lack comprehensive thermodynamic and life cycle assessments (LCA). A more detailed review of fossil-free production pathways for DME can be found with Styring *et al.*[23] Insights into green DME production with a catalytic focus can be found with Alvarez *et al.*,[24] Huang *et al.*,[25] Catizzone *et al.*,[26] and Estevez *et al.*[27] Critically, these alternative feedstock focused studies have been designed and evaluated almost exclusively for steady-state operation and not in the context of flexible operation.

Simultaneously, the traditional core process for DME synthesis has undergone significant innovation. The original indirect synthesis route from fossil-based synthesis gas *via* methanol to DME suffered from thermodynamic limitations and low single-pass yields.[28,29] Although efforts to decarbonize the indirect route have been explored,[30,31] it has largely been

[a]Process Systems Engineering (AVT.SVT), RWTH Aachen University, 52074 Aachen, Germany. E-mail: kaan.rehwasser@rwth-aachen.de

[b]Department of Chemistry and Applied Biosciences, Institute for Chemical and Bioengineering, ETH Zurich, 8093 Zurich, Switzerland

[c]Department of Energy Science and Engineering, Stanford University, 94305 Stanford, California, USA

[d]Institute of Energy Technologies, Electrochemical Process Engineering (IET-4), Forschungszentrum Jülich GmbH, 52428 Jülich, Germany

† These authors contributed equally to this work.

superseded by direct synthesis routes.[31–33] While direct routes improve yields, they often require substantial recycle streams and face challenges with catalyst deactivation due to water formation.[10,34] To mitigate water-formation, *in situ* fixed bed adsorption has emerged, known as Sorption Enhanced DME Synthesis (SEDMES).[16,34–37] SEDMES operates effectively at low pressures and achieves high DME yields, making it the favored method for water removal over membranes.[35,38] Peinado *et al.*[39] provide a comprehensive review of further advancements of the SEDMES process. These advances include the use of pressure-swing regeneration,[40] the introduction of clearing gas to separate CO_2 and DME in the outflow,[41] self-heat recuperation,[42] heteropolyacid catalysts,[43] optimization of catalyst-sorbent particle size[44] and weight ratio,[45] and reactive distillation.[46] Styring *et al.*[47] perform a cradle-to-grave LCA comparing the production and use of gasoline and SEDMES-DME. The authors emphasize the importance of procuring off-shore wind energy compared to the regular European grid mix from an emission avoidance standpoint. These results were confirmed in a comparable analysis by Schreiber *et al.*,[48] however both studies do not further discuss the implications of the intermittency of wind and other renewable resources. Three studies report initial results related to the intermittent or dynamic operation of the SEDMES process. Tyraskis *et al.*[49,50] observe no compromise in overall process performance under lower feed flow conditions as reductions in DME productivity are balanced by improved selectivity. Van Kampen *et al.*[51] include dynamic operation in their multi-reactor model but conclude that the non-linear dynamic process behavior still poses challenges for process control. Both studies point out the potential significance of the SEDMES process for flexible Power-to-X applications, emphasizing the need to evaluate the SEDMES process in the context of flexible operation or intermittent energy sources.

Few studies explore a flexible design paradigm for DME synthesis[8,52,53] – without considering the SEDMES process design. Michailos *et al.*,[52] for example, evaluated a membrane-based process and included a simplified compensation for grid services in their economic analysis. A more detailed study of flexible DME completed by Martin *et al.*[53] proposed a direct DME synthesis route from H_2 and CO_2 using variable solar and wind energy for their electrolyzers, computing the number of electrolyzers required throughout the year amid changing energy availability and rigorously optimizing the process in GAMS.[54] While this work serves as an important initial investigation of flexible DME synthesis, it relies on a coarse monthly temporal resolution, does not consider bidirectional flexibility (*e.g.*, re-electrification and storage[4]), and omits an LCA of the flexible process's carbon intensity.

Furthermore, few studies investigate the role of process design optimization coupled with scheduling optimization to enable flexibility while preventing capital-intensive process designs from becoming economically prohibitive. Only Kofler *et al.*[15] formulate a linear optimization model to optimize the investment and hourly operating decisions of their flexible, direct DME process that is, however, neither sorption-enhanced nor accompanied by a life-cycle analysis. Based on this literature review, a clear research gap emerges for assessing advanced DME synthesis processes in the context of bi-directional flexibility, integrated design and scheduling optimization, high resolution energy availability, and LCA impacts.

Building on our previous work,[55] we address this gap by proposing and evaluating a carbon-negative DME production process capable of bidirectional flexibility. The process design integrates a SEDMES reactor with an Reversible Solid Oxide Cell (RSOC). We employ a rigorous, optimization-based methodology to maximize the flexible process's economic potential under dynamic operation while assessing the process's techno-economic and environmental performance, using multiple hourly-resolved, year-long scenarios to capture real-world energy volatility. This holistic techno-economic analysis (TEA) and LCA is benchmarked against conventional and state-of-the-art reference processes to quantify its economic and environmental advantages.

Below, Section 2 presents the process design, modeling framework, techno-economic and life-cycle assessment methodologies, and the design and scheduling optimization framework. Section 3 evaluates the process's economic and environmental performance, quantifies the value of optimization, analyzes flexible operating strategies, and examines key sensitivities.

2 Methodology

2.1 Process description

The proposed process, shown in Fig. 1, couples a RSOC with a SEDMES process to convert CO_2 and H_2O into DME. The RSOC provides bidirectional conversion between electricity and syngas and, together with short-term storage, decouples the upstream electrochemical step from the continuous downstream DME synthesis. This architecture enables the SEDMES subsystem to operate continuously by absorbing the variability of available renewable power through intermediate syngas production, storage, and re-electrification.

2.1.1 RSOC subsystem and operating modes. In electrolysis cell (EC) mode, renewable electricity drives the co-electrolysis of H_2O and CO_2, supported by the reverse water-gas shift reaction (rWGS) to form syngas. Externally sourced CO_2 at 298 K and 60 bar is throttled to the RSOC pressure of 5 bar, mixed with H_2O, and is superheated to 1086 K using electric heaters and integrated heat recovery. A Yttria-stabilized Zirconia (YSZ) electrolyte is selected for its high O^{2-} conductivity at elevated temperature, with optimal performance in the 970 K to 1170 K range, which simultaneously favors rWGS kinetics and syngas quality.[56–59] The hot effluent containing CO, H_2, CO_2, and H_2O is cooled and flashed to ambient conditions to recover liquid water. The gas phase is compressed to 60 bar and stored at 298 K. Oxygen formed in EC mode is stored at 298 K and 200 bar and can be exported.

In fuel cell (FC) mode, the RSOC re-electrifies stored syngas when electricity is scarce or costly. Stored syngas is expanded and heated to 1173 K at 1 bar. Oxygen is supplied from the tank or purchased if needed. Residual CO and H_2 in the cell exhaust are fully oxidized in an afterburner and the released heat is integrated into process heat sinks. The cooled products are flashed to ambient conditions and routed to the CO_2 and H_2O

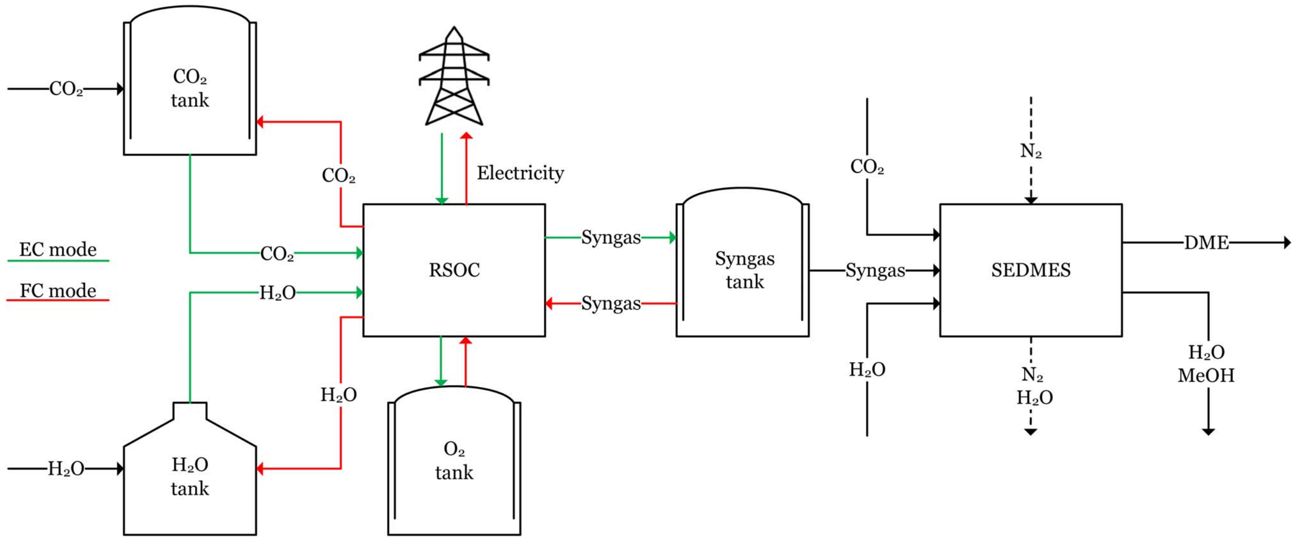

Fig. 1 Overall process design. During renewable energy surplus, the RSOC runs in electrolysis cell (EC) mode (green), turning CO_2 and H_2O into syngas using electricity. This syngas is stored as an intermediate product in a dedicated tank, enabling a constant mass flow to the subsequent steady state SEDMES process. When renewable energy production is low, RSOC switches to fuel cell (FC) mode (red), using syngas to produce electricity.

tanks, closing the material loop. A detailed RSOC flowsheet is provided in the SI (Section S2.2).

2.1.2 SEDMES subsystem and separation. Stored syngas is fed continuously to the SEDMES subsystem (Fig. 2). To shift the reaction equilibrium toward DME, additional CO_2 is co-fed at the reactor inlet.[34] The core unit operation is a temperature-pressure swing adsorption reactor block that enhances water removal capacity compared to single swing reactors. At least three parallel beds enable pseudo-steady DME production: one reactor bed synthesises DME and captures H_2O while the remaining reactor beds undergo H_2O desorption. The operating conditions follow the work of van Kampen *et al.*:[34] DME is synthesised at 548 K and 30 bar. Water desorption occurs at 673 K and 5 bar using nitrogen as a low-cost purge. The water-laden nitrogen is cooled to 312 K and is flashed; the recovered liquid H_2O is used downstream in the distillation section. Given the low cost of N_2 and the additional capital for a recycle loop, N_2 is repurchased rather than recycled.[60]

The reactor effluent enters a compact separation train to purify the DME product. A composite polymer membrane[61]

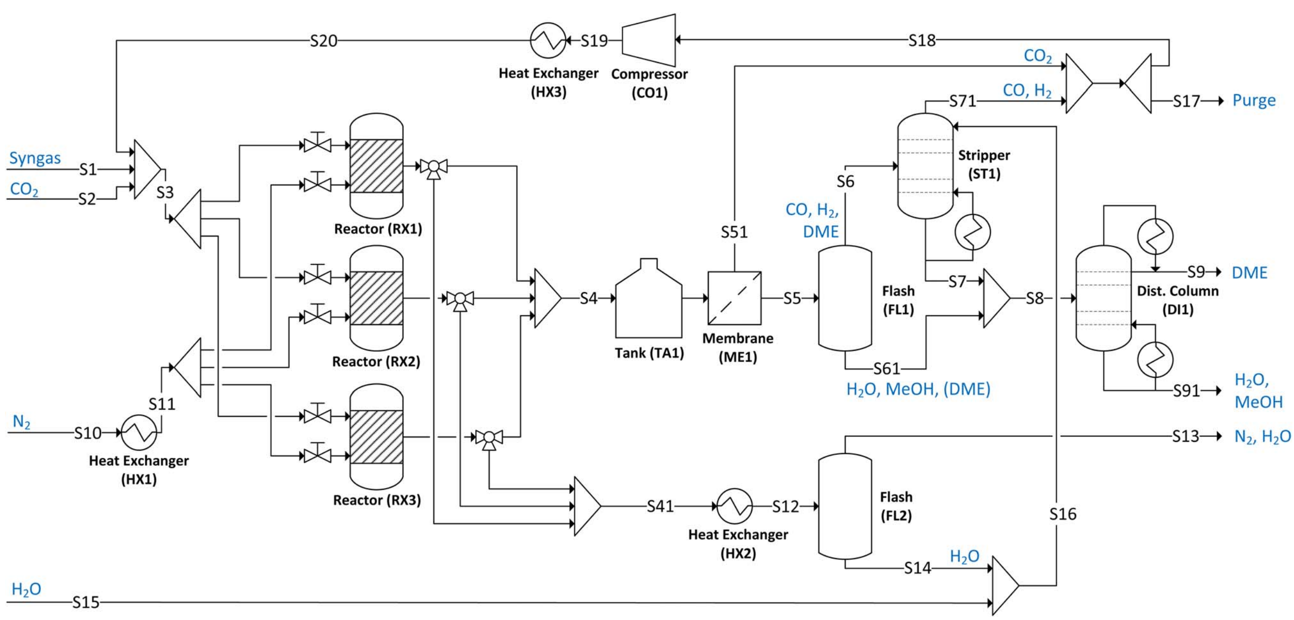

Fig. 2 Flowsheet of the SEDMES subprocess. The N_2 stream is used for water desorption in the reactors. For selected streams, the major components are listed. A detailed stream table is provided in the SI (Section S2.4).

operated at 548 K and 29 bar removes most CO_2. A subsequent flash at 330 K and 29 bar separates methanol and H_2O into the heavy phase, leaving DME mixed with CO, H_2, and residual CO_2 in the light phase. Following Azizi *et al.*,[28] dissolved DME in the light gas is captured in a water absorption column. The remaining CO_2, CO, and H_2 are stripped from the absorbent in a reboiled stripper. The marginal DME remaining in the stripper overhead is recycled and does not measurably affect reactor conversion.[62] The stripper bottoms are combined with the flash bottoms and are sent to a final distillation step that produces 99.50% pure DME in accordance with ISO 16861.[63] The bottoms stream from the distillation column contains 0.6% MeOH and is sent to wastewater treatment.

2.2 Process modeling and simulation

The RSOC and SEDMES subsystems were modeled in Aspen Plus (v12) and Matlab (v2021b) to resolve high-temperature phase behavior, reaction equilibria, and system-level heat and mass integration. For thermodynamics, the PSRK equation of state is used which models polar and non-polar mixtures at high temperatures and pressures.[64] As Aspen Plus does not include electrochemical unit models, the RSOC is represented by a coupled equilibrium and stoichiometric model as implemented by Hauck *et al.*:[58] Two RGIBBS reactors capture the rWGS/WGS chemistry and a single RSTOIC step enforces the electrochemical splitting of H_2O. Mode-specific parameters for EC and FC operation are computed and applied programmatically *via* a Matlab script that switches between operating modes while maintaining overall element balances and energy closure.[65]

As specified, the SEDMES subsystem is fed continuously from the syngas buffer to operate at steady state. The dynamic reactor systems can be averaged as a steady-state reactor system that is modeled as a lumped RSTOIC reactor. To improve stability and convergence of simulations and optimizations, we do not model the SEDMES reactions using kinetic rates but implement conversion rates determined by van Kampen *et al.*[35] through modeling and experiments at identical operating conditions. The resulting CO_2 conversion is 68.1% and further details are provided in the SI (Section S2.3). The true three-bed cyclic configuration is preserved in the techno-economic and life-cycle calculations, where a shortcut sizing model maps operating conditions to reactor dimensions and adsorbent inventory. The mathematical formulation and programmatic files are provided in the SI (Section S2.3).

2.3 Techno-economic modeling

We assess the economic viability of the proposed process using two primary indicators: the net present value (NPV) of the full plant and the levelized break-even price of DME, defined as the constant product price that yields an NPV = 0.

The NPV is calculated by discounting annual cashflows using eqn (1) which accounts for the total capital investment (C_I), annual revenue (R), annual operational costs (C_{OP}) of the plant, as well as plant depreciation (D) and required working capital (C_W) over the plant lifetime (n).[66] t represents the tax rate, and i is the real hurdle rate considering the time value of money and inflation.

$$\mathrm{NPV} = -C_I + (R - C_{OP})\cdot(1-t)\cdot\frac{1-(1+i)^{-n}}{i} + D\cdot t\cdot\frac{1-(1+i)^{-n}}{i} + \frac{C_W}{(1+i)^n} \tag{1}$$

The total capital investment (CAPEX) is obtained by sizing each unit operation and estimating the total installed cost with Guthrie's method.[66] The operational costs (OPEX) include the costs of labor, raw materials, waste disposal, taxes, maintenance, and all utilities (electricity, heating, and cooling). The working capital is calculated to cover one month of accounts receivable, accounts payable, operational costs, and the raw material inventory.[66,67] All key economic assumptions are detailed in Table 1.

2.3.1 Electricity procurement scenarios. To evaluate the behavior and understand trends in the optimal operation of the RSOC-SEDMES plant, three operational scenarios based upon different electricity prices and availability are considered. For each scenario, the economic and environmental performances are calculated and evaluated.

Table 1 Overview of process specifications and assumptions

Parameter	Value
Requirements and specifications of the proposed process	
DME production rate	17 kt year^{-1} (*ca.* 50 t day^{-1})
DME purity	99.50%
DME sales price	1.35 € per kg (ref. 68) (conversion: 1 $: 0.95 €)
Operating hours per year	8160 h year^{-1}
RSOC degradation rate	10% per year (ref. 69)
Plant lifetime	25 Years
Hurdle rate	10%
Tax rate	3%
Depreciation	Linear
CEPCI factor	591.10 (ref. 70)
Purchased carbon dioxide	
CO_2 availability	1 Mt year^{-1} (ref. 71)
CO_2 purity	99.7% (ref. 71)
CO_2 raw material price	40 € per t (ref. 72)
Purchased electricity	
Wind park scenario	Mermaid wind park data for 2021[73] and 52.47 € per MWh (PPA)[74]
Electricity network scenario	Unlimited from grid and Spot market price[73]
Constrained scenario	Mermaid wind park data[73] and spot market price[73]
Purchased nitrogen	
N_2 raw material price	0.25 € per kg
Purchased and sold oxygen	
O_2 raw material price	0.39 € per kg

(1) Wind park scenario: constant contractual electricity price with variable electricity availability of a 600 MW rated wind park[73] (constant price, variable availability).

(2) Electricity network scenario: fluctuating market spot price with non-limiting electricity availability from the French Electricity network[73] (variable price, constant availability).

(3)Constrained scenario: combining the variabilities of scenarios 1 and 2, this case assumes fluctuating market spot prices and variable electricity availability of a 600 MW rated wind park[73] (variable price, variable availability).

The RSOC-SEDMES process is evaluated through a hypothetical plant in Dunkirk, France, set to operate from 2030 onward. This location was selected to co-locate with a planned DMX carbon capture facility, which will provide a 1 Mt year^{-1} source of 99.70% pure CO_2.[71] The plant's renewable energy source is modeled as a planned 600 MW offshore wind farm, with availability based on data from the nearby Mermaid Wind Park[73] at a contractual planned power agreement price of 52.47 € per MWh.[74] The pure oxygen generated by the RSOC EC operation is considered a valuable co-product. This stream is accounted for as such in the economic, environmental (LCA), and thermodynamic (exergetic) process evaluations. Key design specifications (*e.g.*, 17 kt year^{-1} DME production, *etc.*) and all cost assumptions are detailed in Table 1.

2.4 Optimization

To determine the optimal process design and evaluate both economic performance and operational flexibility, the RSOC-SEDMES system is optimized using a sequential two-stage framework. First, a process design optimization (MINLP) identifies the optimal steady-state configuration and sizing of the plant. Second, once the design is fixed, a production scheduling optimization (MILP) is solved to determine the optimal hourly operation under fluctuating energy availability and pricing. This sequential approach decouples the complex thermodynamic design from the computationally intensive time-series scheduling. The scenarios and constraints for both stages are specified in Section 2.3.1 (Table 1).

2.4.1 Process design optimization. The process design optimization is formulated as a black-box mixed-integer nonlinear programming (MINLP) problem to determine the optimal sizing and process parameters of the RSOC-SEDMES process in steady state. Optimal values for the design degrees of freedom (*e.g.*, RSOC temperature, number of distillation trays, *etc.*) are identified *via* a genetic algorithm (GA)[75] that maximizes the NPV of the process within a feasible design space.

Following iterative techniques for black-box process flowsheet optimization,[65] our Aspen Plus process simulation interfaces through the Component Object Model (COM) with custom MATLAB scripts that are used to size and cost each unit operation. Heat integration is considered during optimization *via* a MATLAB pinch-based script. Any iteration where the Aspen Plus model fails to converge is considered infeasible and assigned a significant penalty. A full list of the optimization variables and their bounds is provided in the SI (Section S3).

2.4.2 Flexible operation optimization. To account for the variability in renewable electricity availability and price, a demand-side management (DSM) mixed-integer linear programming (MILP) scheduling problem is solved to optimize the operation of the designed RSOC-SEDMES process. The MILP's objective is to maximize the plant's NPV by determining the optimal operating mode (EC, FC, or idle) and the corresponding syngas/power flow for each hour. The MILP is constrained by the hourly electricity availability (per Section 2.3.1) and considers the variable electricity price, as defined for each electricity scenario in Section 2.3.1. Additional detail and the full mathematical formulation of the MILP are provided in the SI(Section S3.2).

2.4.3 Sensitivity analysis. To assess the robustness of the economic results and of the impact of flexible operation, we perform three complementary sensitivity analyses by perturbing key economic parameters, adjusting electricity price volatility, and re-optimizing for the electricity price and availability of a different year. For the economic parameter sensitivity, eleven parameters are individually adjusted over a range of $\pm$50%, and the break-even price is recomputed for the optimized non-flexible case and each of the three flexible scenarios by re-solving the DSM scheduling problem. To investigate the impact of electricity price volatility, the spot-price distribution is widened about its mean by a range of scaling factors and the flexible operation is re-optimized at each level. Finally, to test the dependence of our results on the chosen year, the scheduling optimization is repeated using the electricity availability and price profiles of 2025 in place of 2021. Throughout these analyses, the plant design obtained from the genetic algorithm is held fixed. The complete parameter list, perturbation ranges, and methodology are provided in the SI (Section S5).

2.5 Greenhouse gas life cycle assessment

The environmental performance of the process was evaluated using a cradle-to-gate life cycle assessment (LCA) quantifying and comparing the greenhouse gas (GHG) emissions of the proposed RSOC-SEDMES process against the reference processes (defined in Section 2.6). The functional unit for the assessment is 1 kg of DME at 99.5% purity. The assessment is based on the Greenhouse gases, Regulated Emissions, and Energy use in Transportation (GREET®) model.[76] We consider the following GHGs: CO_2 (including CO and volatile organic compounds) and the CO_2-equivalents of CH_4 and N_2O. Other environmental impact categories such as acidification, eutrophication, ecotoxicity, water use, land use, or resource depletion are not included in this analysis. The LCA is performed for the first year of operation (2030). The system boundary of our analysis, our treatment of dynamic production, complete LCIs, and additional assumptions are provided in the SI (Section S4.3).

2.6 Definition of comparison processes

To provide a comprehensive performance context, we benchmark our proposed RSOC-SEDMES process against two distinct groups of comparators: (1) established and emerging literature

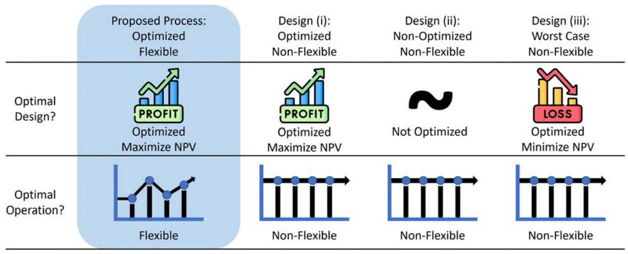

Fig. 3 Overview of the fully optimized design and the three comparative RSOC-SEDMES designs that are used to demonstrate the impact of optimization on the RSOC-SEDMES process design and operation. The blue highlighted design depicts the fully optimized RSOC-SEDMES design proposed in this work.

processes for DME production, and (2) non-flexible and non-optimized variations of the proposed RSOC-SEDMES process itself.

The first group allows us to evaluate the novelty of the process against alternative literature based processes. We select three external reference processes. The first is the state-of-the-art reference, a conventional, fossil-based DME process from natural gas *via* the indirect methanol pathway.[77] The second, a state-of-research benchmark, represents a frequently researched gasification process utilizing biomass.[78] Finally, for a more direct economic comparison to another power-to-X process, we include the E-DME process proposal from Michailos *et al.*,[52] which uses hydrogen from a PEM electrolyzer and captured CO_2 to synthesize DME *via* the indirect synthesis route.

With the second group we determine the value of flexible operation and design optimization by comparing the RSOC-SEDMES process against its own non-optimized baseline designs. We define four internal RSOC-SEDMES process variations, which are depicted in Fig. 3. The primary process is the "Optimized, Flexible Design", which uses the two-stage (MINLP/MILP) optimization to optimize both the process design and the flexible, hourly operation (Section 2.4). This is benchmarked against three non-flexible (steady-state) baselines. The first baseline is the "Optimized, Non-Flexible Design", which still uses the GA-based design optimization to maximize NPV but assumes a constant, steady-state operation of both the RSOC and the SEDMES process. The second baseline is the "Non-Optimized, Non-Flexible Design", which represents a heuristic design and uses a feasible but non-optimized set of design variables operating at steady state. The final case is the "Pessimistic Worst-Case, Non-Flexible Design", which establishes a lower economic bound by using the GA to actively minimize the NPV. A further description of the comparison processes is included in the SI (Section S3.3).

3 Results and discussion

We evaluate the flexible RSOC-SEDMES process from a techno-economic and environmental perspective. In this section, we first present the overall performance of the fully optimized, flexible process across the three electricity scenarios and benchmark these results against the established literature processes defined in Section 2.6. Following this, we quantify the value of flexible process operation and process optimization by comparing the optimized design to the series of internal, non-optimized and non-flexible baselines defined in Section 2.6. Finally, we provide a detailed analysis of the optimal flexible operating regimes to reveal the emergent strategies and dynamic behaviors driving the process performance.

3.1 Overall process performance

3.1.1 Economic performance. The economic performance of the fully optimized, flexible RSOC-SEDMES process across all three electricity scenarios is summarized in Fig. 4. All three scenarios result in negative NPVs at the current market price of DME (1.35 € per kg (ref. 68)). The wind park scenario yields a break-even price of 3.11 € per kg, the electricity network scenario yields 3.54 € per kg, and the constrained scenario yields 3.83 € per kg. Notably, oxygen is a valuable byproduct of the process and is produced at industrial-grade purity in EC mode. In both the wind park and electricity network scenarios, revenues from oxygen sales reduce the break-even price by approximately 20–25%. The contribution of oxygen sales is shown in Fig. 4. Although none of the scenarios are profitable at the current market price, the wind park scenario is the most economically favorable. The analysis of why the wind park scenario has the lowest break even price is discussed in Section 3.3, where the behavior of the different operating regimes is discussed in detail. The design of the fully optimized RSOC-SEDMES process and the comparison processes can be found in the SI (Section S3.4).

When benchmarked against the literature processes, the proposed RSOC-SEDMES process exhibits a higher break-even price than the biomass-based (2.64 € per kg)[81] and E-DME (2.19 € per kg)[52] reference processes. However, a direct comparison between these processes is challenging and must

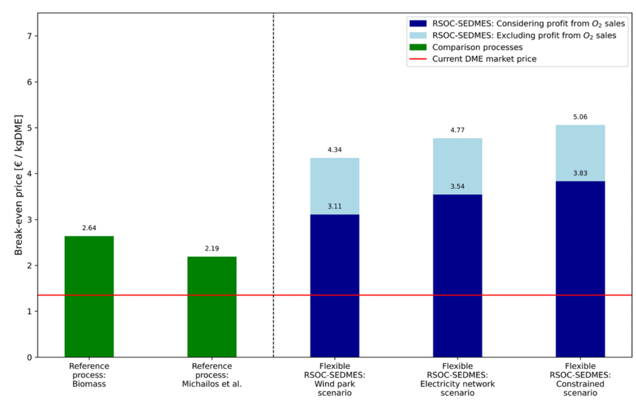

Fig. 4 Comparison of break-even prices as a measure of economic process performance. The horizontal line represents the current market price of DME (1.35 € per kg) produced by the conventional natural gas-based route.[79] Moreover, the proposed RSOC-SEDMES process is compared to a biomass-based pathway[80] and another E-DME pathway by Michailos *et al.*[52]

be considered based on three key factors. First, this work compares a dynamically-operated, flexible process, subject to the constraints of realistic intermittent power, against traditional steady-state literature designs. Second, the reference processes vary significantly in scale. For example, the Michailos *et al.* process has a 15-fold larger production capacity, which provides a significant economy-of-scale advantage. Finally, our analysis deliberately excluded speculative positive financial factors, such as CO_2 taxes or future electrolyzer cost reductions, to maintain a conservative baseline.

3.1.2 Environmental performance. The cradle-to-gate life cycle greenhouse gas (GHG) emissions for the three flexible scenarios are presented in Fig. 5. The Wind Park (Scenario 1) and Constrained (Scenario 3) scenarios, which are both powered primarily by dedicated renewable energy, achieve the same net-negative GHG emissions of -1.96 $kg_{CO_2\ eq}$ per kg_{DME}. The Electricity Network (Scenario 2) has a lesser, though still net-negative, reduction of -1.36 $kg_{CO_2\ eq}$ per kg_{DME}, a direct result of the emissions associated with the French grid-supplied electricity.

When benchmarked against the literature reference processes, all three RSOC-SEDMES scenarios significantly outperform the state-of-the-art fossil-based process (2.07 $kg_{CO_2\ eq}$ per kg_{DME}). Furthermore, the renewable-powered scenarios (1 and 3) also demonstrate a marginally superior environmental impact compared to the state-of-the-research biomass process (-1.81 $kg_{CO_2\ eq}$ per kg_{DME}).

This discrepancy between the scenarios highlights that the overall environmental performance is critically dependent on the electricity source. The superior GHG reduction in Scenarios 1 and 3 is directly attributable to the use of dedicated wind power, whereas the grid emissions in Scenario 2 partially offset the environmental benefit of CO_2 utilization.

For a full life-cycle assessment, emissions from the chemical's use phase must also be considered. Because DME is a bulk chemical with diverse applications, these emissions are not included here. As an illustrative example, combustion of DME as a transportation fuel emits 1.91 $kg_{CO_2\ eq}$ per kg_{DME},[47] resulting in well-to-wheel emissions of at least -0.05 to 0.55 $kg_{CO_2\ eq}$ per kg_{DME} across the considered scenarios, excluding fuel distribution and listed cradle-to-gate omissions (SI, Section S4.3).

Besides the economic and environmental performance metrics, we determine an exergetic efficiency of 50.2%, which clearly outperforms the natural gas-based process. This improvement is primarily driven by extensive heat integration. The detailed methodology and the comparison with the reference processes are provided in the SI (Section S4.2).

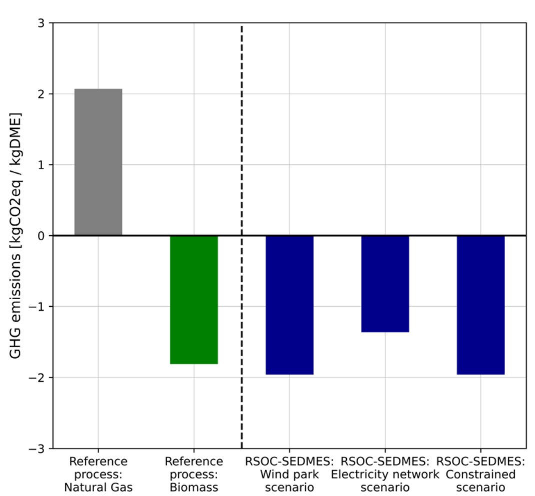

Fig. 5 Comparison of lifetime GHG emissions as a measure of environmental process performance. The proposed RSOC-SEDMES process is compared to a natural gas-based pathway[79] and a biomass-based pathway.[80]

3.2 Techno-economic impact of design optimization and flexibility

The impact of the two-stage optimization strategy is quantified in Fig. 6, which demonstrates that rigorous mathematical optimization substantially improves the economic performance of the process. First, evaluating the black-box MINLP design optimization reveals a dramatic reduction in cost compared to the baselines. The Pessimistic Worst-Case Design establishes the lower bound of performance with a break-even price of 97.88 € per kg. The Non-Optimized "Heuristic" Design, representing a feasible first-guess based on engineering intuition, achieves a break-even price of 7.15 € per kg. By contrast, the Optimized Non-Flexible Design, determined *via* the Genetic Algorithm, achieves a significantly reduced break-even price of 4.27 € per kg. This corresponds to a 96% improvement relative to the worst-case design and a 40% improvement relative to the heuristic baseline, highlighting the critical role of rigorous flowsheet design optimization for this process.

Beyond steady-state design optimization, the DSM MILP scheduling optimization unlocks further value through operational flexibility. When comparing the optimized steady-state design (4.27 € per kg) with the flexible scenarios (3.11–3.83 € per kg), it is evident that enabling flexible operation reduces the production cost by an additional 10–27%. This improvement arises primarily from the system's ability to leverage lower

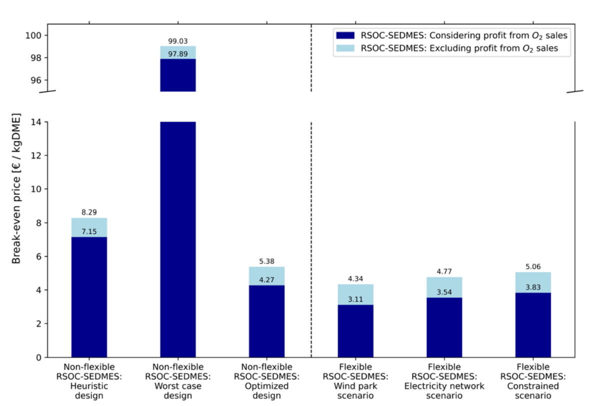

Fig. 6 Economic comparison of internal benchmarks, illustrating the value of design optimization (non-flexible baselines) and operational flexibility (flexible scenarios).

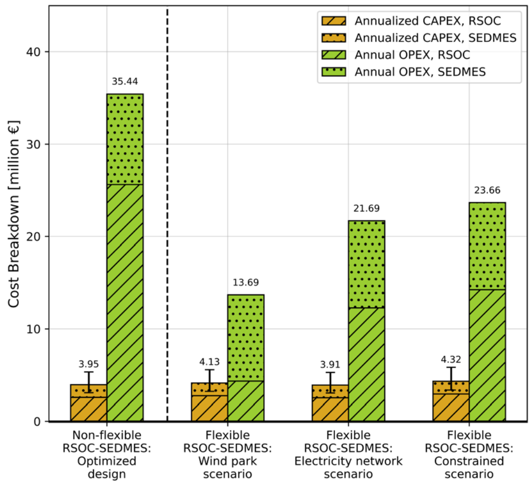

Fig. 7 Comparison of annualized CAPEX and annual OPEX costs between the optimized, non-flexible RSOC-SEDMES process and the optimized, flexible processes. Annualization of CAPEX assumes a 10% discount rate and a 25 years life time. The uncertainty ranges capture the uncertainty associated with the Guthrie-based capital cost estimation method and are assumed to be −22% to +35%.[82] Sensitivities of the OPEX to electricity, oxygen and CO_2 price are analyzed in Section 3.4.

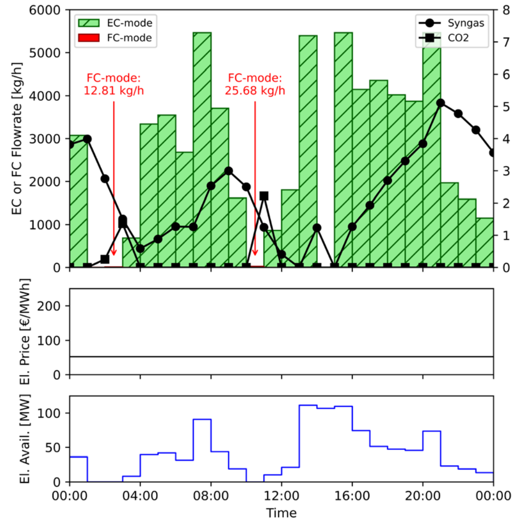

Fig. 8 Optimal RSOC operating regime for the wind park scenario (variable electricity availability, constant electricity price). Data for Jan 02, 2021.

electricity prices-either through a favorable Power Purchase Agreement (Scenario 1) or by dynamically scheduling production during periods of low spot-market prices (Scenarios 2 and 3).

To understand the mechanism behind this improvement, the CAPEX and OPEX of the flexible and non-flexible designs are compared in Fig. 7. From these results, a clear trade-off emerges between the flexible and non-flexible designs. Enabling flexibility requires a marginally higher CAPEX investment to achieve a significantly lower OPEX. In the flexible scenarios, the total CAPEX rises by approximately 1–10% compared to the non-flexible design due to the need for a larger RSOC and syngas storage to preproduce syngas for times of prohibitive electricity cost or availability. However, this increased capital expenditure is overwhelmingly offset by OPEX savings. In Scenario 1, leveraging a low-cost PPA cuts operating costs by 61%, while in Scenarios 2 and 3, the scheduling minimizes OPEX by avoiding high spot-market prices, reducing operational costs by 39% and 33%, respectively. These results illustrate that investing in the capital infrastructure for flexibility pays off by drastically lowering electricity-related expenses.

3.3 Analysis of process behavior under flexible operation

The optimized process exhibits distinct operating behaviors when subjected to variable electricity prices and availabilities. In the wind park scenario (Scenario 1), with variable electricity availability and a constant price, the process operates in EC mode whenever sufficient electricity is available. During times when the available electricity is insufficient to meet the SEDMES process's continuous demand, the RSOC is forced to operate in FC mode to provide the necessary electricity (Fig. 8). As the electricity price is constant, the FC mode is utilized exclusively for intermittency mitigation to maintain continuous chemical production during periods of low wind availability. The wind park scenario achieves the lowest break-even price of the three scenarios, as the contractual PPA price of 52.47 € per MWh is substantially below the average spot-market price, reducing OPEX significantly. This cost advantage is reduced by a marginal increase in CAPEX required to store additional syngas for periods of low wind availability (Fig. 7).

In the electricity network scenario (Scenario 2), with non-limiting electricity and a variable price, the MILP optimization identifies a strategy based on shifting production to low-cost periods. Surplus syngas is produced during times of low electricity prices, allowing the RSOC process to run idle during periods with high electricity prices (Fig. 9). An equilibrium

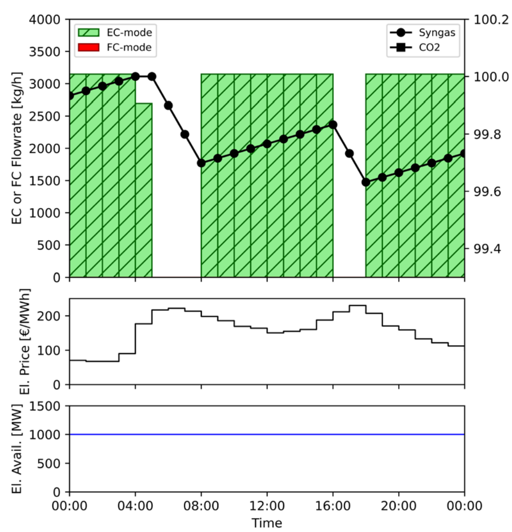

Fig. 9 Optimal RSOC operating regime for the electricity network scenario (non-limited electricity availability, variable electricity price). Data for Oct 04, 2021.

exists between the cost savings from this flexible scheduling and the additional CAPEX required for a larger syngas tank. The electricity-generating FC mode is never used, as the observed price spread ($\text{price}_{\text{max}} - \text{price}_{\text{min}} = 686.18$ € per MWh) is insufficient or occurs too infrequently to justify the additional capital investment of a larger RSOC and storage tank.

In the constrained scenario (Scenario 3), which features both variable availability and variable price, characteristics from the first two scenarios are observed. Similarly to the wind park scenario, the process operates in EC mode while sufficient electricity is available to produce a syngas buffer for periods of insufficient electricity. This mode, however, is additionally influenced by variable electricity price and the optimizer therefore preferentially concentrates EC operation during low-price hours, following a similar strategy to the electricity network scenario. The optimizer therefore balances the cost of a larger RSOC subsystem enabling greater syngas production at low-price hours against the benefit of reduced electricity expenditure, subject to the additional constraint of limited wind availability. As in the electricity network scenario, the FC mode is not used for grid export at the present price spread, as discussed further in Section 3.4.2.

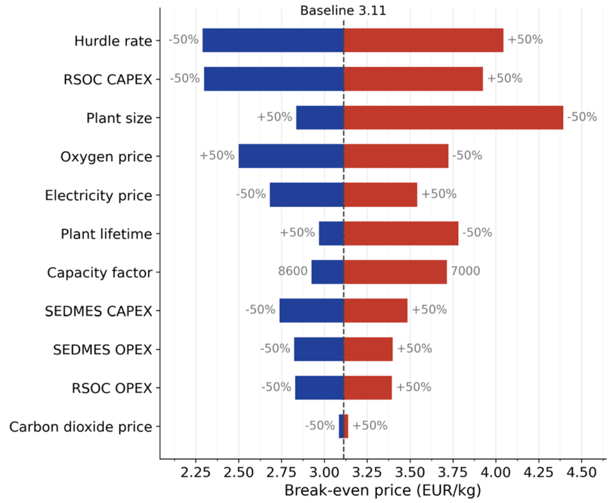

Fig. 11 Tornado plot of the break-even price sensitivity for the flexible wind park scenario. Labels at the ends of each row depict the degree of perturbation or the range of values investigated in the sensitivity analysis.

3.4 Sensitivity analysis

The results of the three sensitivity analyses reveal that the benefit of flexible operation over steady-state operation is consistent across all analyses. The magnitude of the benefit and the mechanisms driving it, however, vary by analysis, as discussed in the following subsections.

3.4.1 Economic parameter sensitivity. Across all eleven perturbed economic parameters, flexible operation reduces the break-even price relative to steady-state operation, with the benefit ranging from 19.1–34.4% with a baseline of 27.2% (Fig. 10). The corresponding break-even prices range from 2.29–4.39 € per kg with a baseline of 3.11 € per kg (Fig. 11). The flexibility benefit is most sensitive to the hurdle rate, oxygen price, and plant size, while the break-even price is most sensitive to the hurdle rate, RSOC CAPEX, and plant size. Across the perturbed parameters, the flexibility benefit and break-even price are in some cases correlated and in others inversely correlated. The RSOC CAPEX, for example, is the second-largest driver of the absolute break-even price but has negligible impact on the flexibility benefit, as it burdens the flexible and non-flexible designs to a similar degree. The electricity price affects both metrics inversely. A lower price reduces the break-even price but also reduces the flexibility benefit, as the value of flexible scheduling is greatest when there are high prices to avoid. The hurdle rate has the most significant positive impact, simultaneously reducing the break-even price and increasing the benefit of flexible operation. A lower hurdle rate increases the present value of the long-term OPEX savings (*cf.* Fig. 7), amplifying its economic advantage over the non-flexible case.

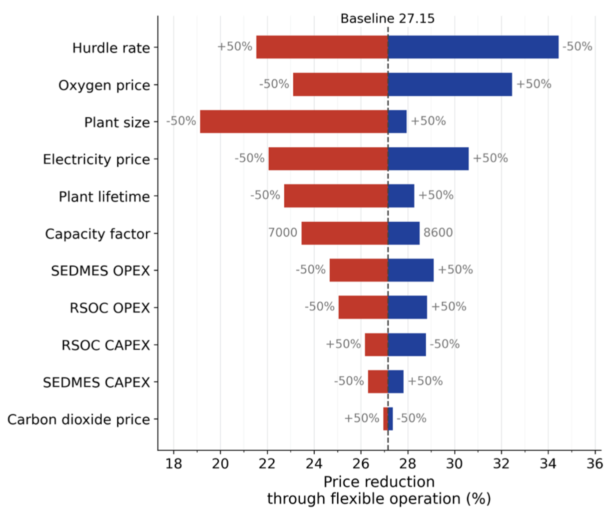

Fig. 10 Tornado plot of the percent reduction in break-even price observed between the optimal, non-flexible design and the optimal flexible design under the wind park scenario. Labels at the ends of each row depict the degree of perturbation or the range of values investigated in the sensitivity analysis.

The break-even price falls substantially under favorable financing or reduced RSOC capital cost, reaching 2.29 € per kg and a 34.4% benefit from flexible operation at a hurdle rate of 5%, which approaching the cost of the literature reference processes. These results indicate that with policy-supported financing, as is common for first-of-a-kind decarbonisation assets, combined with the RSOC cost reductions anticipated as the technology matures, flexibly produced carbon-negative DME could become economically viable. All data and additional analysis of the results and assumptions is provided in the SI (Section S5.1).

3.4.2 Electricity price volatility sensitivity. At the present price volatility, the flexible RSOC-SEDMES process does not generate any additional value through electricity exports to the grid and captures its economic advantage entirely through load-shifting and self-supplying electricity. Notably however, once the price spread widens beyond roughly 1.5× its current value, the optimization identifies a strategy where the FC is actively used to export electricity to the grid at times of peak prices (Fig. S11), with the electricity-network and constrained scenarios exporting 0.52 GWh year^{-1} and 0.21 GWh year^{-1} respectively. The lower export volume in the constrained scenario reflects its limited wind availability, which restricts the syngas inventory available for re-electrification. Beyond a spread of approximately 2×, electricity sales revenue exceeds the RSOC operating cost, structurally improving the process economics. The exported volume and RSOC capacity grow steadily with further widening until the RSOC stack reaches its maximum output of 43.4 MW at approximately 6× the current spread, beyond which additional volatility increases export hours rather than peak power. As day-ahead price volatility is widely expected to increase with rising variable-renewable penetration, the plant retains a latent grid-balancing option that would activate under more volatile market conditions. The complete results across all spread levels are provided in the SI (Section S5.2, Tables S6 and S7).

3.4.3 Electricity availability and price profile sensitivity. Re-optimizing the DSM scheduling problem for the 2025 electricity availability and price profile confirms the benefit of flexible operation across all three scenarios, while revealing a reordering of the scenario ranking driven by the lower prevailing electricity price. Flexible operation reduces the break-even price relative to steady-state operation by 11.8%, 17.7%, and 10.9% for the wind park, electricity network, and constrained scenarios, with break-even prices of 3.13 € per kg, 2.92 € per kg, and 3.16 € per kg, respectively. The wind park scenario behaves similarly to the 2021 result, as the wind availability profiles of the two years are comparable. These results indicate that while the qualitative finding of flexible operation's economic advantage is robust across years, the relative ranking of the electricity procurement scenarios is sensitive to the prevailing electricity price level and therefore should be interpreted in the context of the prevailing electricity market conditions.

The most consequential difference between the 2021 and 2025 solutions is the lower average electricity price in 2025 (61.5 € per MWh against 109.2 € per MWh in 2021), which reorders the electricity procurement scenario ranking. The electricity network scenario achieves the lowest break-even price at 2.92 € per kg, in contrast to the wind park scenario in the 2021 base case. Two effects drive this reordering. At an average spot price of 61.5 € per MWh, the fixed power purchase agreement of 52.47 € per MWh confers considerably less advantage than at 2021 prices, significantly reducing the benefit of operating under a planned power purchase agreement. Conversely, the electricity network scenario benefits directly from the lower electricity prices, as the scheduling optimization concentrates production in the cheapest hours, achieving an effective electricity cost below the PPA rate, which was not possible in 2021. The constrained scenario performs worst, as its limited wind availability forces the process to purchase grid electricity even when doing so is financially disadvantageous. These results indicate that while the qualitative finding of flexible operation's economic advantage is robust across years, the relative ranking of the electricity procurement scenarios is sensitive to the current electricity price level and therefore should be interpreted in the context of the prevailing electricity market conditions.

4 Conclusion

This work proposes a novel process design for sustainable dimethyl ether (DME) production, specifically engineered to utilize captured CO_2 and adapt to the fluctuating costs and availability of renewable energy sources. The design integrates a reversible solid oxide cell with a sorption-enhanced DME synthesis process to enable bi-directional flexibility, ensuring continuous production despite intermittent energy supply. A comprehensive model of the process was created by interfacing Aspen Plus and MATLAB, allowing for a rigorous assessment *via* an MINLP process design optimization and a MILP demand-side management optimization.

The optimized process demonstrates competitive performance across three real-world case studies (wind park, electricity network, constrained) in terms of economic, environmental, and thermodynamic indicators. The economic performance is measured *via* the break-even price of DME, which ranges from 3.11 € per kg (wind park scenario) to 3.83 € per kg (constrained scenario). While these costs remain higher than current fossil benchmarks, the economic competitiveness could be improved *via* future reductions in electrochemical cell costs, rising natural gas prices, or policy-driven incentives for CO_2 reduction. The environmental impact is minimized through the utilization of captured carbon. The process achieves net-negative cradle-to-gate GHG emissions of $-1.96\ \mathrm{kg_{CO_2\ eq}}$ per $\mathrm{kg_{DME}}$ in the renewable-dominated scenarios (wind park & constrained scenario) and $-1.36\ \mathrm{kg_{CO_2\ eq}}$ per $\mathrm{kg_{DME}}$ in the electricity network scenario. This represents a substantial improvement over the natural gas-based state-of-the-art process in all scenarios and a slight improvement over the biomass-based state-of-research process in most scenarios.

Additionally, this work quantifies the impact of optimization-based process development for flexible systems. Using a genetic algorithm to optimally design the RSOC-SEDMES process enhances its economic performance by 40% relative to a nominal heuristic design and 96% relative to a worst-case baseline. Furthermore, identifying the optimal flexible production regime by employing strategies such as load shifting and intermittency mitigation improves the economic performance by a further 27% relative to the optimized non-flexible configuration. This improvement is achieved by balancing the increased capital investment required for flexibility against the resulting saved operational expenditures. Consequently, this analysis illustrates that utilizing sequential design and scheduling optimization can be an effective strategy for mitigating the economic risks associated with novel flexible processes.

This work is subject to several limitations that future research should address. The transient operation of both the RSOC and the novel SEDMES process are topics of ongoing research and not fully reflected in the presented conversion-based modeling approach. Similarly, while degradation is accounted for through a fixed annual degradation rate of 10%, the model does not link degradation to the actual cycling frequency resulting from flexible operation and may therefore underestimate cycling-induced wear. In addition, practical factors such as operational constraints, material and energy losses are not fully represented in the process model.

In summary, the proposed RSOC-SEDMES process establishes a robust pathway for the utilization of captured CO_2 and intermittent renewable energy to produce sustainable DME. Beyond the specific production of DME, this study highlights the potential of evolving beyond traditional steady-state design paradigms toward flexible, dynamic operation. As the chemical industry transitions toward renewable feedstocks, the integration of operational flexibility and rigorous optimization, as demonstrated in this work, will become increasingly essential for ensuring the economic competitiveness of sustainable chemical processes.

Author contributions

DJ, MH: conceptualization, methodology, software, investigation, formal analysis, visualization, validation, writing – original draft, writing – review & editing; JB, JG, JP: conceptualization, methodology, software, investigation, formal analysis, visualization, writing – original draft; KR: conceptualization, methodology, validation, project administration, writing – review & editing, supervision.

Conflicts of interest

The authors declare no conflicts of interest.

Data availability

All data software files supporting the findings of this study, including process simulations, optimization scripts, and life cycle assessment models, are openly available in Zenodo at: https://doi.org/10.5281/zenodo.15338006.

Supplementary information (SI): supplementary materials are available for this publication and include details on the process design, process modeling, optimization formulation, thermodynamic, economic, and LCA analyses, as well as our screening method to identify flexible, carbon-utilizing chemical processes. See DOI: https://doi.org/10.1039/d6se00114a.

Acknowledgements

The authors thank Alexander Mitsos and Simone Mucci for their valuable feedback. We acknowledge funding from the Bio-Based Industries Joint Undertaking GreenSolRes under the European Union's Horizon 2020 research and innovation program under grant agreement No. 720695 (GreenSolRes).

Notes and references

1 A. Mitsos, N. Asprion, C. A. Floudas, M. Bortz, M. Baldea, D. Bonvin, A. Caspari and P. Schaefer, *Comput. Chem. Eng.*, 2018, **113**, 209–221.
2 A. Kätelhön, R. Meys, S. Deutz, S. Suh and A. Bardow, *Proc. Natl. Acad. Sci. U. S. A.*, 2019, **116**, 11187–11194.
3 C. Ganzer and N. Mac Dowell, *Sustain. Energy Fuels*, 2020, **4**, 3888–3903.
4 J. Burre, D. Bongartz, L. C. Bree, K. Roh and A. Mitsos, *Chem. Ing. Tech.*, 2020, **92**, 74–84.
5 G. J. Fulham, P. V. Mendoza-Moreno and E. J. Marek, *Energy Environ. Sci.*, 2024, **17**, 4594–4621.
6 E. Catizzone, G. Bonura, M. Migliori, F. Frusteri and G. Giordano, *Molecules*, 2018, **23**, 31.
7 M. A. Charalambous, V. Tulus, M. W. Ryberg, J. Pérez-Ramírez and G. Guillén-Gosálbez, *Sustain. Energy Fuels*, 2023, **7**, 1930–1941.
8 D. Bongartz, L. Doré, K. Eichler, T. Grube, B. Heuser, L. E. Hombach, M. Robinius, S. Pischinger, D. Stolten, G. Walther and A. Mitsos, *Appl. Energy*, 2018, **231**, 757–767.
9 A. Linzenich, K. Arning, D. Bongartz, A. Mitsos and M. Ziefle, *Appl. Energy*, 2019, **249**, 222–236.
10 S. Guffanti, C. G. Visconti, J. van Kampen, J. Boon and G. Groppi, *Chem. Eng. J.*, 2021, **404**, 126573.
11 A. M. Parvez, I. M. Mujtaba, P. Hall, E. H. Lester and T. Wu, *Energy Technol.*, 2016, **4**, 526–535.
12 G. De França Lopes, L. Bonfim-Rocha, L. M. De Matos Jorge and P. R. Paraíso, *Bioenergy Res.*, 2020, **13**, 397–410.
13 M. Tomatis, A. Mahmud Parvez, M. T. Afzal, S. Mareta, T. Wu, J. He and T. He, *Fuel*, 2019, **254**, 115627.
14 R. Kofler and L. R. Clausen, *Energy Convers. Manage.*, 2023, **281**, 116815.
15 R. Kofler, N. Campion, M. Hillestad, W. Meesenburg and L. R. Clausen, *Energy Fuels*, 2024, **38**, 8777–8803.
16 G. Skorikova, M. Saric, S. N. Sluijter, J. van Kampen, C. Sánchez-Martínez and J. Boon, *Front. Chem. Eng.*, 2020, **2**, 1–11.
17 M. N. DinAli and I. Dincer, *J. Energy Resour. Technol.*, 2019, **141**, 122003.
18 M. De Falco, G. Natrella, M. Capocelli, P. Popielak, M. Sołtysik, D. Wawrzyńczak and I. Majchrzak-Kucęba, *Energies*, 2022, **15**, 3516.
19 G. Botta, M. Solimeo, P. Leone and P. V. Aravind, *Fuel Cells*, 2015, **15**, 669–681.
20 T.-W. Wu and I.-L. Chien, *Chem. Eng. Res. Des.*, 2022, **177**, 1–12.
21 M. Matzen and Y. Demirel, *J. Clean. Prod.*, 2016, **139**, 1068–1077.
22 M. Pozzo, A. Lanzini and M. Santarelli, *Fuel*, 2015, **145**, 39–49.
23 P. Styring, G. R. M. Dowson and I. O. Tozer, *Front. Energy Res.*, 2021, **9**, 663331.
24 A. Álvarez, A. Bansode, A. Urakawa, A. V. Bavykina, T. A. Wezendonk, M. Makkee, J. Gascon and F. Kapteijn, *Chem. Rev.*, 2017, **117**, 9804–9838.
25 M.-H. Huang, H.-M. Lee, K.-C. Liang, C.-C. Tzeng and W.-H. Chen, *Int. J. Hydrogen Energy*, 2015, **40**, 13583–13593.
26 E. Catizzone, C. Freda, G. Braccio, F. Frusteri and G. Bonura, *J. Energy Chem.*, 2021, **58**, 55–77.

27 R. Estevez, L. Aguado-Deblas, F. M. Bautista, F. J. López-Tenllado, A. A. Romero and D. Luna, *Catalysts*, 2022, **12**, 1555.
28 Z. Azizi, M. Rezaeimanesh, T. Tohidian and M. R. Rahimpour, *Chem. Eng. Process. Process Intensif.*, 2014, **82**, 150–172.
29 C. Mevawala, Y. Jiang and D. Bhattacharyya, *Appl. Energy*, 2015, **204**, 163–180.
30 M. A. Adnan and N. I. Fajar Mukti, *Renewable Energy*, 2026, **256**, 124043.
31 M. Kanso, J. Boon, A. Capa, L. Tiruta-Barna and C. E. Robles-Rodriguez, *Front. Chem. Eng.*, 2026, **8**, 1796275.
32 A. Hankin and N. Shah, *Sustain. Energy Fuels*, 2017, **1**, 1541–1556.
33 V. Dieterich, K. Neumann, A. Niederdränk, H. Spliethoff and S. Fendt, *Energy*, 2024, **301**, 131688.
34 J. van Kampen, J. Boon, J. Vente and M. van Sint Annaland, *J. CO2 Util.*, 2020, **37**, 295–308.
35 J. van Kampen, J. Boon and M. van Sint Annaland, *J. Mater. Chem. A*, 2021, **9**, 14627–14629.
36 J. van Kampen, J. Boon, J. Vente and M. van Sint Annaland, *React. Chem. Eng.*, 2021, **6**, 244–257.
37 D. Liuzzi, C. Peinado, M. A. Peña, J. van Kampen, J. Boon and S. Rojas, *Sustain. Energy Fuels*, 2020, **4**, 5674–5681.
38 H. Li, S. Ren, S. Zhang, S. Padinjarekutt, B. Sengupta, X. Liang, S. Li and M. Yu, *J. Mater. Chem. A*, 2021, **9**, 2678–2682.
39 C. Peinado, D. Liuzzi, S. N. Sluijter, G. Skorikova, J. Boon, S. Guffanti, G. Groppi and S. Rojas, *Chem. Eng. J.*, 2024, **479**, 147494.
40 J. Van Kampen, S. Booneveld, J. Boon, J. Vente and M. Van Sint Annaland, *Chem. Commun.*, 2020, **56**, 13540–13542.
41 V. Dikić, L. Zubeir, M. Sarić and J. Boon, *Separations*, 2023, **10**, 403.
42 Y. Kansha, M. Ishizuka, C. Song and A. Tsutsumi, *Energy*, 2015, **90**, 122–127.
43 C. Peinado, D. Liuzzi, J. Boon and S. Rojas, *Catal. Today*, 2025, **455**, 115319.
44 S. Renda, J. Soler, J. Herguido and M. Menéndez, *Biomass Bioenergy*, 2025, **197**, 107764.
45 S. Guffanti, C. G. Visconti and G. Groppi, *Ind. Eng. Chem. Res.*, 2021, **60**, 6767–6783.
46 C. S. Bîldea, R. Győrgy, C. C. Brunchi and A. A. Kiss, *Comput. Chem. Eng.*, 2017, **105**, 142–151.
47 P. Styring, P. W. Sanderson, I. Gell, G. Skorikova, C. Sánchez-Martínez, G. Garcia-Garcia and S. N. Sluijter, *Front. Sustain.*, 2022, **3**, 1057190.
48 A. Schreiber, S. Troy, S. Weiske, R. C. Samsun, R. Peters, P. Zapp and W. Kuckshinrichs, *J. CO_2 Util.*, 2024, **82**, 102743.
49 I. Tyraskis, A. Capa, G. Skorikova, S. N. Sluijter and J. Boon, *Front. Chem. Eng.*, 2025, **7**, 1521374.
50 I. Tyraskis, A. Capa, G. Skorikova, S. N. Sluijter and J. Boon, *Ind. Chem. Mater.*, 2026, **4**, 244–259.
51 J. Van Kampen, J. Overbeek, J. Boon and M. Van Sint Annaland, *Front. Chem. Eng.*, 2023, **5**, 1055896.
52 S. Michailos, S. McCord, V. Sick, G. Stokes and P. Styring, *Energy Convers. Manage.*, 2019, **184**, 262–276.
53 M. Martín, *J. CO2 Util.*, 2016, **13**, 105–113.
54 GAMS Development Corporation, *General Algebraic Modeling System (GAMS), Release 27.3*, Fairfax, VA, USA, 2019.
55 J. Bothe, J. Güttler, M. Heyer, D. Jakobs, J. Pavšek and K. Karacasulu, *CO_2 Utilization under Intermittent Electricity Supply: Sorption Enhanced DME Synthesis with an Integrated RSOC Process, Rwth Aachen University, Eurecha Committee Eurecha Student Contest Report*, 2022.
56 V. M. Schmidt, *Elektrochemische Verfahrenstechnik*, Wiley, 2003.
57 V. Venkataraman, M. Pérez-Fortes, L. Wang, Y. S. Hajimolana, C. Boigues-Muñoz, A. Agostini, S. J. McPhail, F. Maréchal, J. van herle and P. V. Aravind, *J. Energy Storage*, 2019, **24**, 100782.
58 M. Hauck, S. Herrmann and H. Spliethoff, *Int. J. Hydrogen Energy*, 2017, **42**, 10329–10340.
59 F. Bustamante, R. M. Enick, A. V. Cugini, R. P. Killmeyer, B. H. Howard, K. S. Rothenberger, M. V. Ciocco, B. D. Morreale, S. Chattopadhyay and S. Shi, *AIChE J.*, 2004, **50**, 1028–1041.
60 C. Styles, Costs of nitrogen gas – how much should you be paying?, 2017, https://puritygas.ca/nitrogen-gas-costs/.
61 A. Brunetti, F. Scura, G. Barbieri and E. Drioli, *J. Membr. Sci.*, 2010, **359**, 115–125.
62 Merck KGaA, Dimethylether, https://www.sigmaaldrich.com/DE/de/substance/dimethylether4607115106.
63 International Organization for Standardization, *Petroleum Products - Fuels (Class F) - Specifications of Dimethyl Ether (DME)*, 2010.
64 Aspen Technology Inc, *Physical Property Methods and Models 11.1*, 2001.
65 U. Lee, J. Burre, A. Caspari, J. Kleinekorte, A. M. Schweidtmann and A. Mitsos, *Ind. Eng. Chem. Res.*, 2016, **55**, 12014–12026.
66 L. Biegler, I. Grossmann, A. Westerberg and Z. Kravanja, *Systematic Methods of Chemical Process Design*, Prentice Hall PTR, 1997.
67 W. D. Seider, D. R. Lewin, J. D. Seader, S. Widagdo, R. Gani and K. M. Ng, *Product and Process Design Principles: Synthesis, Analysis and Evaluation, 4th Edition*, Wiley, 2004.
68 Business Analytiq, Dimethyl ether price index, 2024, https://businessanalytiq.com/procurementanalytics/index/dimethyl-ether-price-index/.
69 F. Marino, G. Loreti, M. Della Pietra, V. Cigolotti, G. Monteleone and E. Jannelli, *Int. J. Hydrogen Energy*, 2026, **220**, 154111.
70 Access Intelligence, Chemical Engineering: Economic Indicator, 2022, https://ic.nipc.ir/ic/Portals/0/Introduce/costindex/ChemicalEngineeringVol127%239Sep2020.pdf.
71 DMX Demonstration Dunkirk, *3D Project*, 2022, https://3d-ccus.com/3d-overview/.
72 European Comission, Project description: DMX Demonstration in Dunkirk, 2024, https://cordis.europa.eu/project/id/838031.
73 ENTSO-E, *Transparency Platform*, 2021, https://transparency.entsoe.eu.

74 LevelTen Energy, Q4 2021 PPA Price Index, 2021, https://www.leveltenenergy.com/post/q4-2021.
75 The MathWorks Inc., *MATLAB Optimization Toolbox*, Natick, MA, USA, 2019, https://www.mathworks.com/matlabcentral/answers/414438-how-do-i-cite-matlab-in-a-bibliography-or-a-published-journal.
76 Argonne National Laboratory, GREET: Greenhouse gases, Regulated Emissions, and Energy use in Transportation, 2021, https://greet.es.anl.gov/greet_excel_model.models.
77 U. Lee, J. Han, M. Wang, J. Ward, E. Hicks, D. Goodwin, R. Boudreaux, P. Hanarp, H. Salsing, P. Desai, E. Varenne, P. Klintbom, W. Willems, S. L. Winkler, H. Maas, R. de Kleine, J. Hansen, T. Shim and E. Furusjö, *SAE Int. J. Fuels Lubr.*, 2016, **9**, 546–557.
78 N. Lecksiwilai, S. H. Gheewala, M. Sagisaka and K. Yamaguchi, *J. Clean. Prod.*, 2016, **134**, 523–531.
79 C. Bin, J. Hongguang and G. Lin, *Int. J. Energy Res.*, 2008, **32**, 722–734.
80 A. M. Parvez, T. Wu, S. Li, N. Miles and I. M. Mujtaba, *Biomass Bioenergy*, 2018, **110**, 105–113.
81 F. M. Baena-Moreno, M. Gonzalez-Castaño, H. Arellano-García and T. Reina, *Energy*, 2021, **225**, 120230.
82 AACE International, *Cost Estimate Classification System – as Applied in Engineering, Procurement, and Construction for the Process Industries, AACE International Recommended Practice 18R-97*, 2005.